

Contents lists available at ScienceDirect

Petroleum Science

journal homepage: www.keaipublishing.com/en/journals/petroleum-science



Original Paper

Two exact first-order k-space formulations for low-rank viscoacoustic wave propagation on staggered grids



Hong-Yu Zhou ^a, Yang Liu ^{a, b, *}, Jing Wang ^a

- ^a China University of Petroleum (Beijing), State Key Laboratory of Petroleum Resources and Prospecting and CNPC Key Laboratory of Geophysical Prospecting, Beijing, 102249, China
- ^b China University of Petroleum (Beijing), Karamay Campus, Karamay, Xinjiang, 834000, China

ARTICLE INFO

Article history:
Received 20 January 2022
Received in revised form
2 September 2022
Accepted 18 October 2022
Available online 22 October 2022

Edited by Jie Hao

Keywords: Viscoacoustic K-space Staggered-grid Low-rank

ABSTRACT

Wave propagation in the viscoacoustic media is physically dispersive and dissipated. Completely excluding the numerical dispersion error from the physical dispersion in the viscoacoustic wave simulation is indispensable to understanding the intrinsic property of the wave propagation in attenuated media for the petroleum exploration geophysics. In recent years, a viscoacoustic wave equation characterized by fractional Laplacian gains wide attention in geophysical community. However, the firstorder form of the viscoacoustic wave equation, often solved by the conventional staggered-grid pseudospectral method, suffers from the numerical dispersion error in time due to the low-order finitedifference approximation. It is challenging to completely eliminate the error because the viscoacoustic wave equation contains two temporal derivatives, which stem from the time stepping and the amplitude attenuation terms, respectively. To tackle the issue, we derive two exact first-order k-space viscoacoustic formulations that can fully exclude the numerical error from the physical dispersion. For the homogeneous case, two formulations agree with the viscoacoustic analytical solution very well and have the same efficiency. For the heterogeneous case, our second k-space formulation is more efficient than the first one because the second formulation significantly reduces the number of the wavenumber-space mixed-domain operators, which are the expensive part of the viscoacoustic k-space simulation. Numerical cases validate that the two first-order k-space formulations are effective and efficient alternatives to the current staggered-grid pseudospectral formulation for the viscoacoustic wave simulation.

© 2022 The Authors. Publishing services by Elsevier B.V. on behalf of KeAi Communications Co. Ltd. This is an open access article under the CC BY license (http://creativecommons.org/licenses/by/4.0/).

1. Introduction

Wave propagation simulation in real media (Carcione, 2007; Moczo et al., 2014; Igel, 2017) plays a significant role in geophysical modeling (Alkhalifah, 2000; Carcione et al., 2002; Berkhout, 2014a; De Basabe et al., 2016; Gong et al., 2018; Du et al., 2020; Zou et al., 2020; Xu et al., 2021; Zhou et al., 2021a; Wang et al. 2022a, 2022b) and inversion (Virieux and Operto, 2009; Berkhout, 2014b). Field data (McDonal et al., 1958; Campillo et al., 1985; Yoshimoto et al., 1993) demonstrate that seismic wave propagation in the realistic subsurface suffers from amplitude decay and phase dispersion effects due to the friction induced energy conversion. Researchers name the intrinsic attenuation property in acoustic approximation as viscoacoustic phenomenon (Aki and Richards, 2002; Carcione,

* Corresponding author. E-mail address: wliuyang@vip.sina.com (Y. Liu). 2007). Many theories are formulated to describe the phenomenon (Carcione et al., 1988; Robertsson et al., 1994; Blanch et al., 1995; Zhu and Harris, 2014). Among them, the constant-Q based viscoacoustic theory (McDonal et al., 1958; Kjartansson, 1979; Day and Minster, 1984; Emmerich and Korn, 1987; Zhu and Harris, 2014) is proven to be practical and widely applied to describe acoustic wave propagation in attenuated media.

Generally, there are two main categories that describe the constant-Q viscoacoustic effects, i.e., mechanical superposition based physical models and pure mathematical models. The mechanical superposition models (Liu et al., 1976; Day and Minster, 1984; Blanch et al., 1995; Hestholm and Ruud, 1998; Zhu et al., 2013; Qu and Li, 2019; Qu et al., 2021; Wang and Qu, 2021) combine several springs and dashpots elements connected in series and/or in parallel in a complex way to approximate the frequency independent Q property within certain frequency bands. An alternative category of describing the constant-Q behavior is based on strict mathematical derivations (Kjartansson, 1979), yielding

elegant and simple constant-Q model that only requires parameterization by reference velocity and Q. The model strictly captures the constant-Q behavior for all frequency bands. Typical examples are constant-Q wave equations based on fractional temporal derivatives (Carcione et al., 2002) and fractional spatial derivatives (Carcione, 2010; Treeby and Cox, 2010; Xing and Zhu, 2019). Recently, the fractional spatial derivatives based method (Zhu and Harris, 2014) has gained wide attention from the geophysical community because of two major advantages. First, it avoids previous wavefield storage, which is often the case of the fractional temporal derivative based method (Carcione et al., 2002). Second, the fractional spatial derivatives based method decouples the amplitude decay and phase dispersion effects, facilitating attenuation compensation in seismic imaging (Zhu et al., 2014; Zhu and Harris, 2015).

Accurately and efficiently solving the fractional spatial derivative based viscoacoustic wave equation (Zhu and Harris, 2014) is widely studied in recent years. Unfortunately, the viscoacoustic wave equation, which is often solved by the conventional pseudospectral method (Fornberg, 1987; Özdenvar and McMechan, 1996), suffers from the temporal dispersion error due to the discretization of the time stepping and amplitude attenuation terms. Chen et al. (2016) suppress the temporal dispersion by approximating the original fractional order viscoacoustic wave equation (Zhu and Harris, 2014) using constant fractional derivatives. Wang et al. (2020) design a simplified k-space method by adopting different time stepping error compensation operators for the amplitude decay and phase distortion terms, respectively. However, the numerical dispersion error cannot be fully compensated by these methods (Chen et al., 2016; Wang et al., 2020) because they only approximate the dispersion relation of the original fractional derivative based viscoacoustic wave equation (Zhu and Harris, 2014). Sun et al. (2015) propose eliminating the temporal dispersion by the analytical wavefields based low-rank one-step method, which may increase the storage and computational requirement because of the complex number operations. Notice that the aforementioned temporal dispersion suppressing schemes (Sun et al., 2015; Chen et al., 2016; Wang et al., 2020) focus on the secondorder viscoacoustic wave equation, which may not be easy to account for the density variation and incorporate the perfectly matched layer (PML) (Berenger, 1994; Collino and Tsogka, 2001; Komatitsch and Martin, 2007) based absorbing boundary layers as the first-order one. Besides, compared with the second-order wave equation, the first-order one, solved by the staggered-grid method (Virieux, 1986; Özdenvar and McMechan, 1996; Wang et al. 2021, 2022a; Zhou et al. 2021b, 2022), can effectively remove the artifact caused by the pseudospectral method (Özdenvar and McMechan, 1996). In this paper, we derive two first-order time domain viscoacoustic formulations that can fully exclude the dispersion error from the viscoacoustic wave simulation by the k-space theory (Tabei et al., 2002; Firouzi et al., 2012). Because of the features, we name the new methods as exact first-order k-space formulations. For homogeneous media, our formulations are free from grid dispersion and highly accurate because our derivations are based on the exact dispersion relation of the viscoacoustic wave equation (Zhu and Harris, 2014). For heterogeneous media, we adopt the low-rank method (Engquist and Ying, 2009; Fomel et al., 2013) to accurately represent the mixed-domain operators caused by Q and velocity heterogeneity. Numerical examples demonstrate that our two exact k-space formulations are effective and efficient alternatives to the current pseudospectral method based first-order viscoacoustic formulation.

2. Theory and method

2.1. Conventional first-order staggered-grid pseudospectral formulation of viscoacoustic wave equation

In this part, we summarize the shortcomings of the conventional first-order staggered-grid pseudospectral solver for the fractional derivative based viscoacoustic wave equation. First, we derive the first-order viscoacoustic wave equation from the second-order one (Zhu and Harris, 2014), which has the form

$$\frac{1}{v^2} \frac{\partial^2 u}{\partial t^2} = \tau \frac{\partial}{\partial t} \left(-\nabla^2 \right)^{\gamma + 1/2} u + \eta \left(-\nabla^2 \right)^{\gamma + 1} u, \tag{1}$$

where $u=u(\mathbf{x},t)$ is the pressure wavefield and $\mathbf{x}=(x,z)$ is the position related vector; ∇^2 is the Laplace operator, $v=v_0\cos(\pi\gamma/2)$, $\tau=-v_0^{2\gamma-1}\omega_0^{-2\gamma}\sin(\pi\gamma)$, $\eta=-v_0^{2\gamma}\omega_0^{-2\gamma}\cos(\pi\gamma)$, $\gamma=\arctan(1/Q)/\pi$ and v_0 is the wave propagation velocity defined at reference angular frequency ω_0 . Transforming Eq. (1) into the wavenumber-frequency ($\mathbf{k}-\omega$) domain, we have

$$(i\omega)^2 - v^2 \tau |\mathbf{k}|^{2\gamma + 1} i\omega - v^2 \eta |\mathbf{k}|^{2\gamma + 2} = 0,$$
 (2)

in which $\mathbf{k} = (k_{\rm x}, k_{\rm z})$. Multiplying $\mathbf{k} - \omega$ domain wavefield $U(\mathbf{k}, \omega)$ on both sides of equation, we have

$$(i\omega)^{2}U(\mathbf{k},\omega)+v^{2}\left(\tau|\mathbf{k}|^{2\gamma-1}i\omega+\eta|\mathbf{k}|^{2\gamma}\right)\left(-|\mathbf{k}|^{2}\right)U(\mathbf{k},\omega)=0. \tag{3}$$

Because of the Fourier relations of $i\omega \leftrightarrow \frac{\partial}{\partial t}$ and $-|\mathbf{k}|^2 \leftrightarrow \nabla \cdot \nabla$, in which ∇ is the gradient operator $\nabla = \left(\frac{\partial}{\partial x}, \frac{\partial}{\partial \overline{z}}\right)^T$, Eq. (3) can be expressed in the space—time domain as

$$\frac{\partial^2}{\partial t^2} u + v^2 \left(\tau (-\nabla)^{2\gamma - 1/2} \frac{\partial}{\partial t} + \eta (-\nabla)^{2\gamma} \right) \nabla \cdot \nabla u = 0.$$
 (4)

By defining $\mathbf{v} = (v_x, v_z) = -\frac{1}{\rho} \nabla u$ and $p = \frac{\partial u}{\partial t}$, in which ρ is the density, Eq. (4) can be reformulated into the first-order equations:

$$\frac{\partial p}{\partial t} = \rho v^2 \left(\tau \left(-\nabla^2 \right)^{\gamma - 1/2} \frac{\partial}{\partial t} + \eta \left(-\nabla^2 \right)^{\gamma} \right) \left(\frac{\partial \nu_x}{\partial x} + \frac{\partial \nu_z}{\partial z} \right), \tag{5a}$$

$$\frac{\partial v_{x}}{\partial t} = -\frac{1}{\rho} \frac{\partial p}{\partial x},\tag{5b}$$

$$\frac{\partial v_Z}{\partial t} = -\frac{1}{\rho} \frac{\partial p}{\partial z}.$$
 (5c)

Compared with second-order viscoacoustic wave equation, the first-order viscoacoustic wave equation can simultaneously account for attenuation effect and density variation. Besides, the first-order viscoacoustic wave equation facilitates the implementation of PML (Berenger, 1994; Collino and Tsogka, 2001; Komatitsch and Martin, 2007). Conventionally, the first-order wave equations are often solved by the pseudospectral staggered-grid method (Özdenvar and McMechan, 1996), which gives the discrete form

$$\partial_{t} p(\mathbf{x}, t) = \rho v^{2} \left(\tau \left(-\nabla^{2} \right)^{\gamma - 1/2} \partial_{t}^{-} + \eta \left(-\nabla^{2} \right)^{\gamma} \right) \\
\times \left(\partial_{x}^{-} \nu_{x}(\mathbf{x}_{1}, t) + \partial_{z}^{-} \nu_{z}(\mathbf{x}_{2}, t) \right), \tag{6a}$$

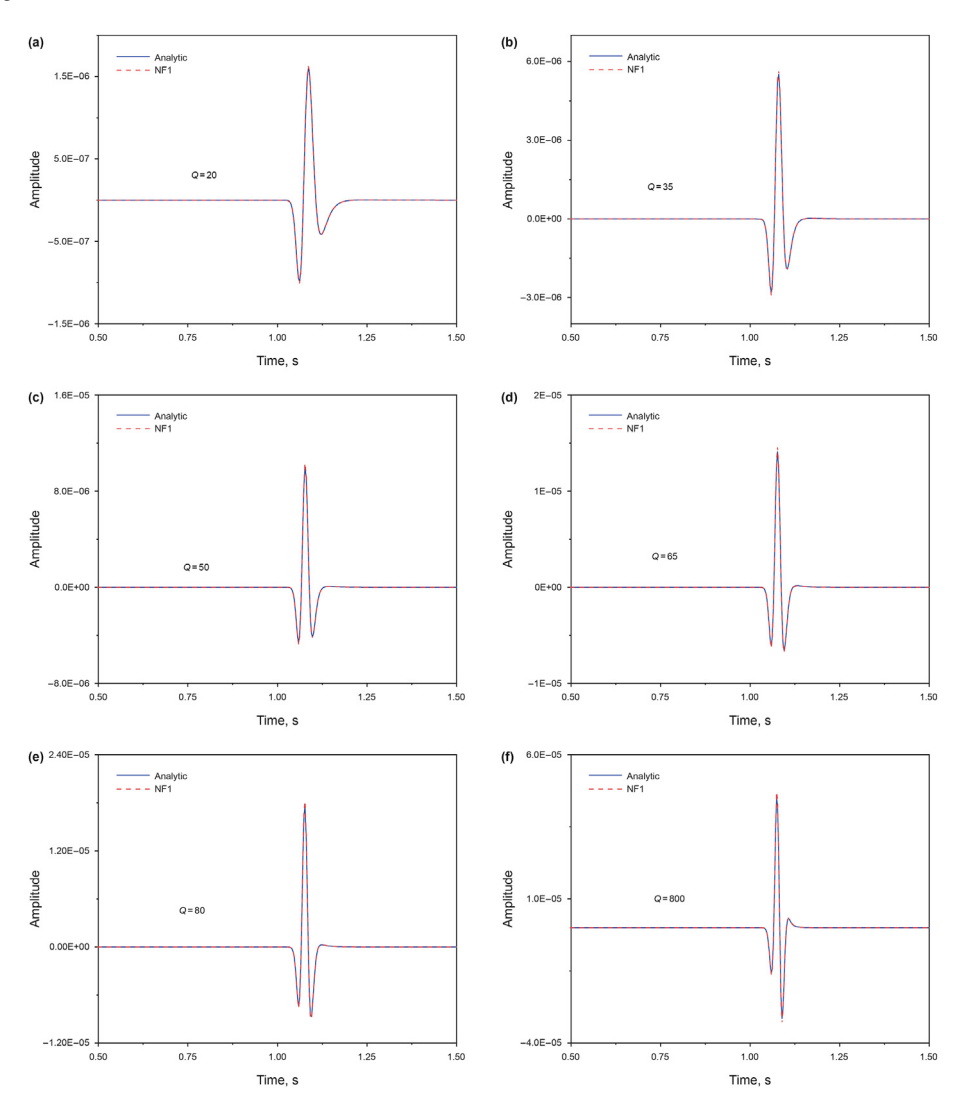


Fig. 1. The numerical solution of NF1 and analytic solution. (a) Q = 20; (b) Q = 35; (c) Q = 50; (d) Q = 65; (e) Q = 80; (f) Q = 80. The receiver is 2200 m away from the 25 Hz Ricker wavelet source with 0.08 s delay. The grid spacing, time step and velocity are 10 m, 3 ms and 2200 m/s, respectively. The density is 2123 kg/m³.

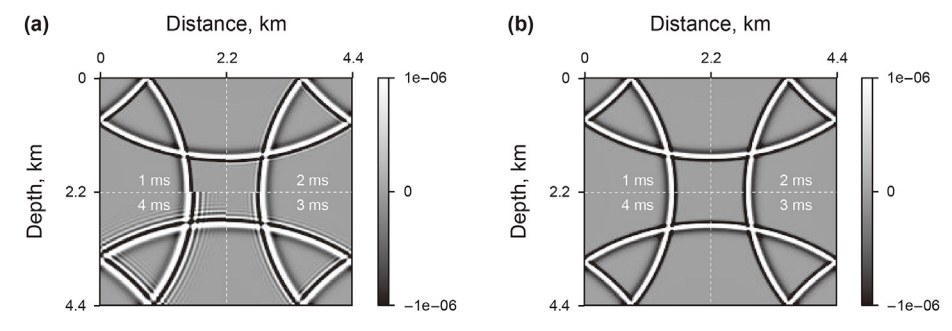


Fig. 2. Snapshots of (a) conventional PS and (b) NF1 in homogeneous velocity and Q media. The velocity and Q are 2200 m/s and 30, respectively. The density is 2123 kg/m³. The grid spacing is 22 m. 22 Hz Ricker wavelet is located at the center of the model. The snapshots are at 1.8 s.

$$\partial_t \nu_X(\mathbf{x}_1, t + \delta t / 2) = -\frac{1}{\rho} \partial_X^+ p(\mathbf{x}, t + \delta t / 2), \tag{6b}$$

 ∂_t^- , ∂_x^+ , ∂_x^- , ∂_z^+ and ∂_z^- can be expressed by space-time dependent variables g(x,t) as

$$\partial_t \nu_z(\mathbf{x}_2, t + \delta t / 2) = -\frac{1}{\rho} \partial_z^+ p(\mathbf{x}, t + \delta t / 2), \qquad (6c) \qquad \partial_t g(\mathbf{x}, t) = \frac{g(\mathbf{x}, t + \delta t / 2) - g(\mathbf{x}, t - \delta t / 2)}{\delta t}, \qquad (7a)$$

in which $\mathbf{x}_1 = (x + \delta x/2, z)$ and $\mathbf{x}_2 = (x, z + \delta z/2)$; the operators ∂_t ,

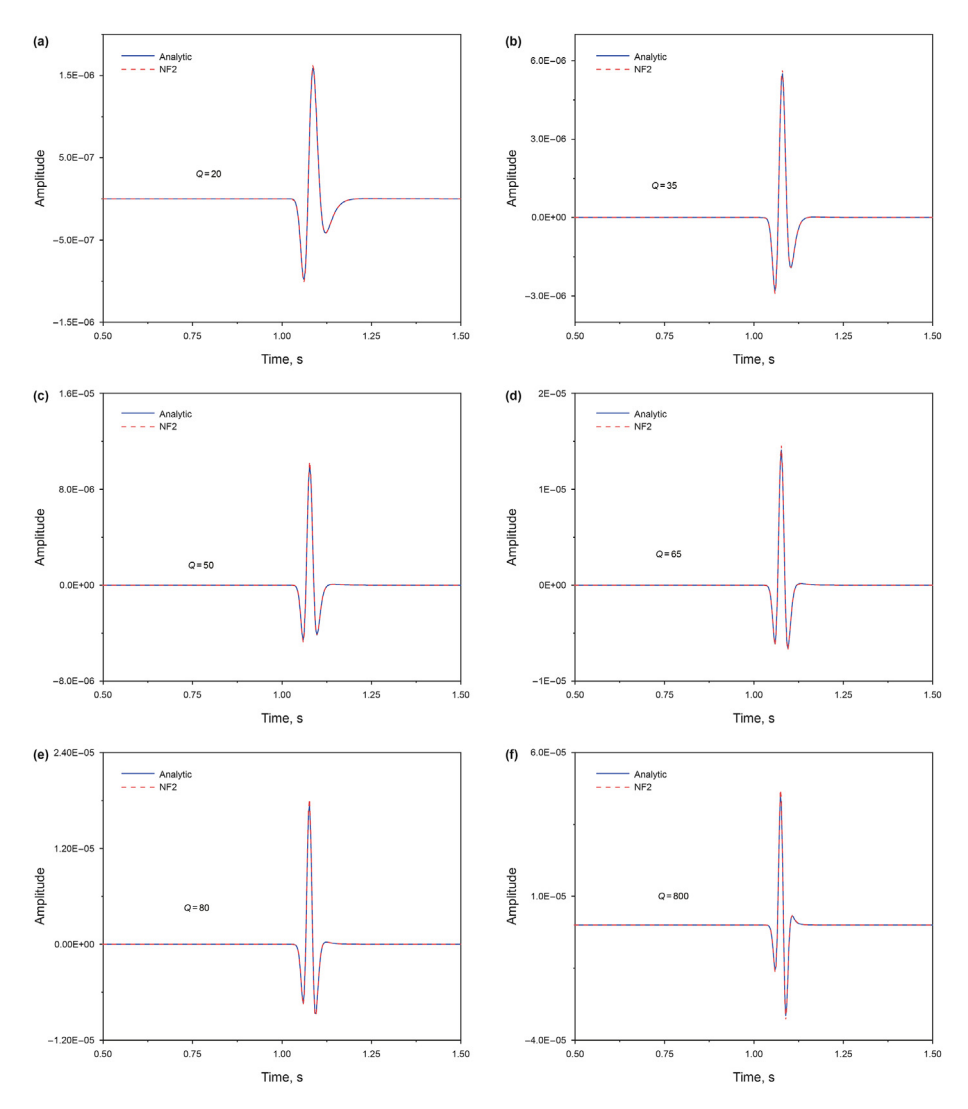


Fig. 3. The numerical solution of NF2 and analytic solution. (a) Q = 20; (b) Q = 35; (c) Q = 50; (d) Q = 65; (e) Q = 80; (f) Q = 80. The receiver is 2200 m away from the 25 Hz Ricker wavelet source, which is with 0.08 s delay. The grid spacing, time step and velocity are 10 m, 3 ms and 2200 m/s, respectively.

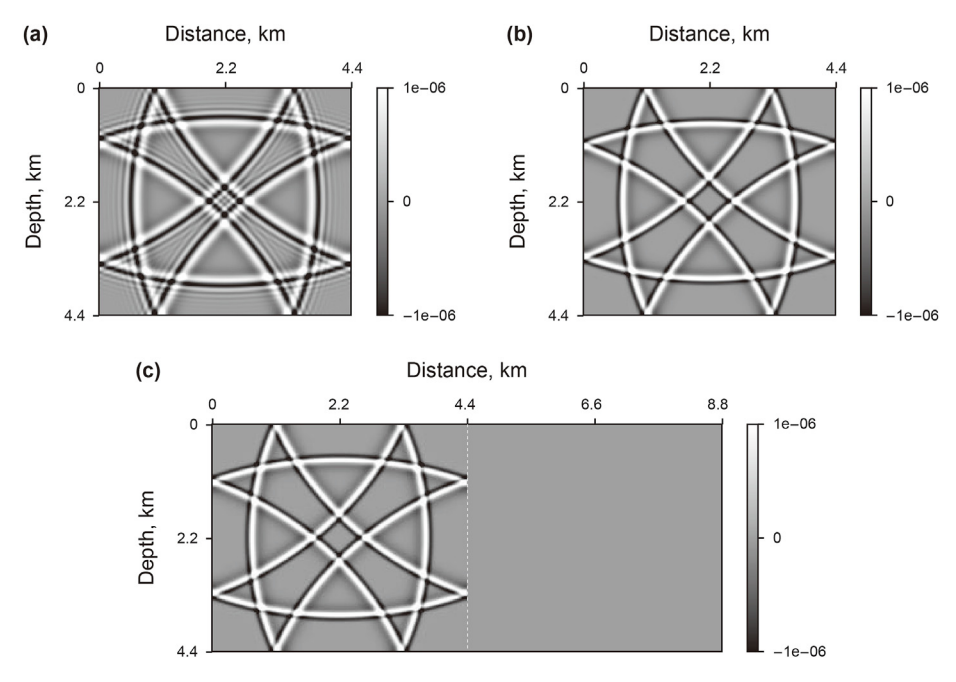


Fig. 4. Snapshots of the conventional PS, NF1 and NF2 in homogeneous velocity and Q media. (a) PS; (b) NF2; the left half of (c) is NF1; the right half of (c) is the snapshot difference of NF1 and NF2. The velocity and Q are 2200 m/s and 30, respectively. The density is 2123 kg/m³. The grid spacing is 22 m. 22 Hz Ricker wavelet is located at the center of the model. The time step is 4 ms. The snapshots are at 2.8 s.

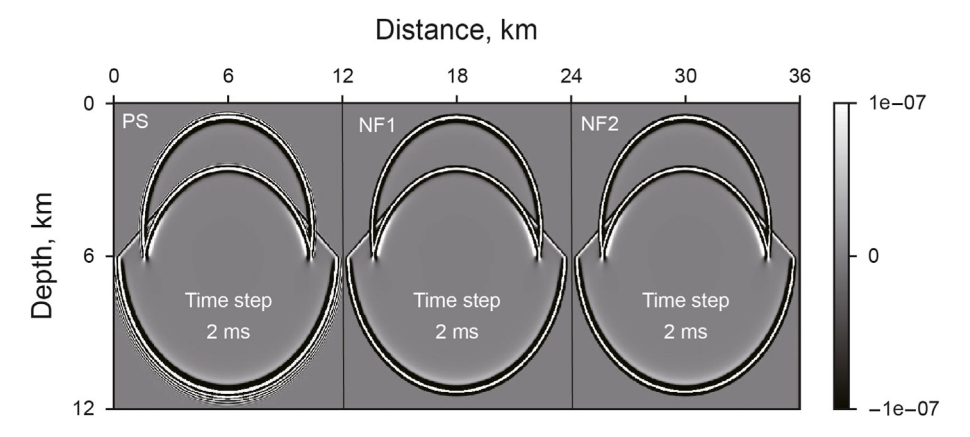


Fig. 5. The snapshots of the PS, NF1 and NF2 methods. The same time step 2 ms is adopted for all methods.

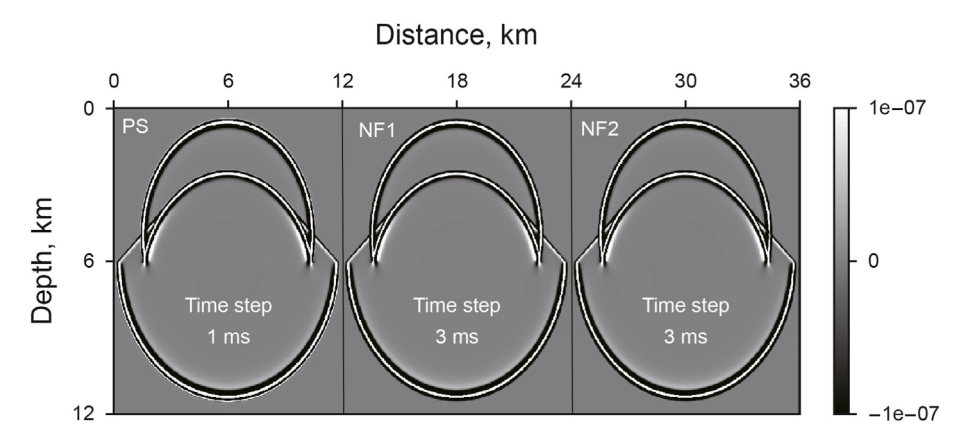


Fig. 6. The snapshots of the PS, NF1 and NF2. The time step for NF1 and NF2 is 3 ms. The PS method breaks down when adopting such a time step. We use the time step 1 ms for the PS method for comparison.

$$\partial_t^- g(\mathbf{x}, t) = \frac{g(\mathbf{x}, t) - g(\mathbf{x}, t - \delta t)}{\delta t}, \tag{7b}$$

$$\partial_{x}^{+}g(\boldsymbol{x},t) = \mathcal{F}^{-1}\left[e^{\mathrm{i}k_{x}\delta x/2}\mathrm{i}k_{x}\mathcal{F}[g(\boldsymbol{x},t)]\right],\tag{7c}$$

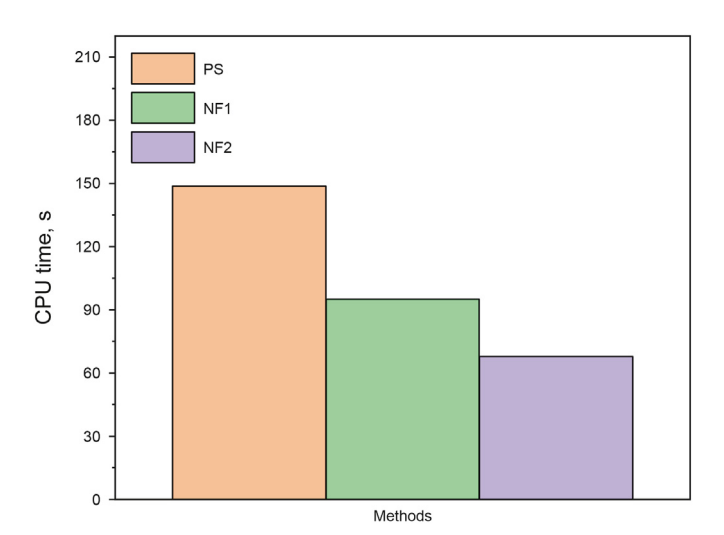


Fig. 7. CPU time of the PS, NF1 and NF2. We compare the CPU time of different methods under the condition of comparable accuracy. The time steps for PS, NF1 and NF2 are 1 ms, 3 ms and 3 ms, respectively.

$$\partial_{x}^{-}g(\mathbf{x},t) = \mathcal{F}^{-1}\left[e^{-\mathrm{i}k_{x}\delta x/2}\mathrm{i}k_{x}\mathcal{F}[g(\mathbf{x},t)]\right],\tag{7d}$$

$$\partial_z^+ g(\boldsymbol{x},t) = \mathcal{F}^{-1} \left[e^{ik_z \delta z/2} ik_z \mathcal{F}[g(\boldsymbol{x},t)] \right], \tag{7e}$$

$$\partial_{z}^{-}g(\boldsymbol{x},t) = \mathcal{F}^{-1}\left[e^{-\mathrm{i}k_{z}\delta z/2}\mathrm{i}k_{z}\mathcal{F}[g(\boldsymbol{x},t)]\right],\tag{7f}$$

where \mathscr{F} and \mathscr{F}^{-1} represent the forward and inverse Fourier transforms in space, respectively. The space-wavenumber domain pseudo-differential operators $(-\nabla^2)^{\gamma-1/2}$ and $(-\nabla^2)^{\gamma}$ can be approximated by separable representation methods (Chen and Liu, 2004; Zhang and Zhang, 2009) such as low-rank matrix decomposition (Engquist and Ying, 2009; Fomel et al., 2013). Because only second-order accuracy center finite-difference operators ∂_t and first-order accuracy backward finite-difference operators ∂_t are applied to approximate the partial derivatives in the discrete wave equation, the overall accuracy of the conventional staggered-grid pseudospectral formulation (6) is only first-order accuracy in time. Coarse time step may distort the waveform for this conventional formulation. Besides, the simulation stability is limited due to the pseudospectral method in this formulation.

2.2. New first-order staggered-grid formulation of viscoacoustic wave equation: formulation 1

To tackle the aforementioned problems, we propose a new first-order staggered-gird formulation for the viscoacoustic wave

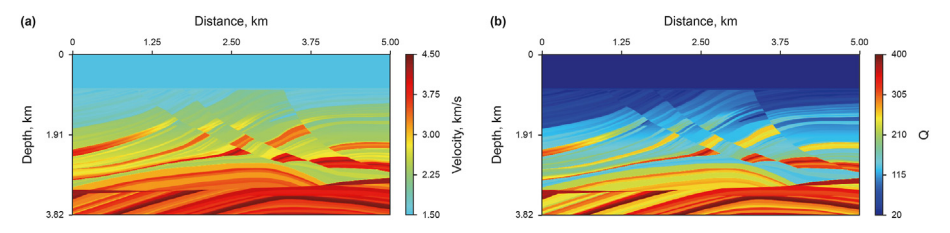


Fig. 8. (a) Velocity and (b) Q models. The reference frequency is 50 Hz. The density is calculated by the empirical formula $\rho = 310v^{0.25}$. The grid spacing is 10 m.

equation. We derive the new formulation from the k-space theory (Bojarski, 1982; Tabei et al., 2002; Firouzi et al., 2012), and name it new formulation 1 (NF1) for short.

In appendix A, we have derived the k-space time marching form for viscoacoustic case as

$$= \frac{\frac{U(\boldsymbol{k},t+\delta t) - 2U(\boldsymbol{k},t) + U(\boldsymbol{k},t-\delta t)}{\delta t^2}}{\delta t^2} + \frac{U(\boldsymbol{k},t)2\left(e^{-\frac{b}{2}\delta t}\cos\left(\frac{\sqrt{4c-b^2}}{2}\delta t\right) - 1\right)}{\delta t^2} + \frac{U(\boldsymbol{k},t-\delta t)\left(1 - e^{-b\delta t}\right)}{\delta t^2}.$$
(8)

One can reformulate Eq. (8) into the equivalent first-order equations:

$$\begin{split} &\frac{P(\boldsymbol{k},t+\delta t/2)-P(\boldsymbol{k},t-\delta t/2)}{\delta t}\\ &=-\rho v^2(\widehat{\partial}_X V_X(\boldsymbol{k},t)+\widehat{\partial}_Z V_Z(\boldsymbol{k},t))+\frac{P(\boldsymbol{k},t-\delta t/2)\Big(e^{-b\delta t}-1\Big)}{\delta t}, \end{split} \tag{9a}$$

$$\frac{V_{x}(\mathbf{k},t+\delta t)-V_{x}(\mathbf{k},t)}{\delta t}=-\frac{1}{\rho}\widehat{\partial}_{x}P(\mathbf{k},t+\delta t/2), \tag{9b}$$

$$\frac{V_{z}(\mathbf{k}, t + \delta t) - V_{z}(\mathbf{k}, t)}{\delta t} = -\frac{1}{\rho} \widehat{\vartheta}_{z} P(\mathbf{k}, t + \delta t / 2), \tag{9c}$$

in which $P(\boldsymbol{k},t) = \frac{U(\boldsymbol{k},t+\delta t/2)-U(\boldsymbol{k},t-\delta t/2)}{\delta t}, \ V_X(\boldsymbol{k},t) = -\frac{1}{\rho}\widehat{\partial}_X U(\boldsymbol{k},t)$ and $V_Z(\boldsymbol{k},t) = -\frac{1}{\rho}\widehat{\partial}_Z U(\boldsymbol{k},t); \ \widehat{\partial}_X = \mathrm{i} k_X \sqrt{L}, \ \widehat{\partial}_Z = \mathrm{i} k_Z \sqrt{L}$ and $L = \frac{2e^{-\frac{b}{2}\delta t}\cos\left(\frac{\sqrt{4c-b^2}}{2}\delta t\right)-e^{-b\delta t}-1}{-|\boldsymbol{k}|^2 v^2 \delta t^2}.$

Solving Eqs. (9a)-(9c) by staggered-grid pseudospectral method (Özdenvar and McMechan, 1996) in space-time domain, we have NF1 as

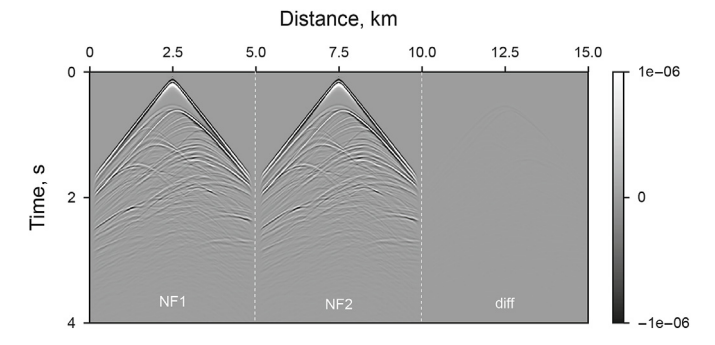


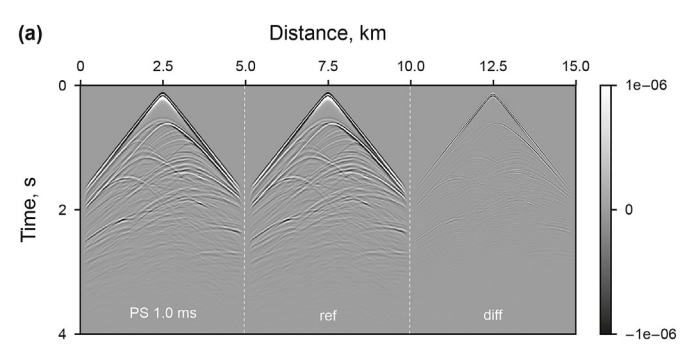
Fig. 9. Seismic records of NF1, NF2 and their difference. The rank and time step for both methods are 4 and 1.4 ms, respectively. The annotation "diff" means the difference between the seismic records of NF1 and NF2.

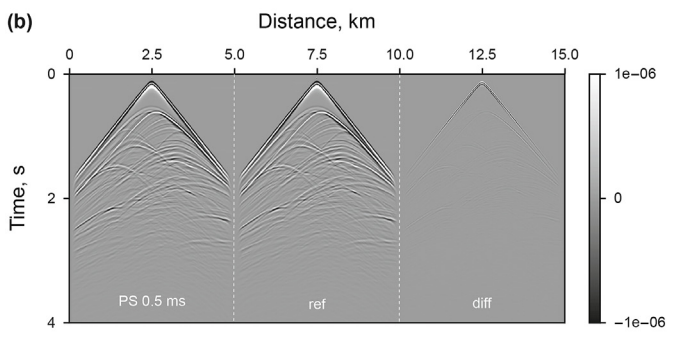
$$\partial_t p(\mathbf{x}, t) = -\rho v^2 \left(\tilde{\partial}_X^- \nu_X(\mathbf{x}_1, t) + \tilde{\partial}_Z^- \nu_Z(\mathbf{x}_2, t) \right) + \partial_S p(\mathbf{x}, t - \delta t / 2), \tag{10a}$$

$$\partial_t \nu_X(\mathbf{x}_1, t + \delta t / 2) = -\frac{1}{\rho} \tilde{\partial}_X^+ p(\mathbf{x}, t + \delta t / 2), \tag{10b}$$

$$\partial_t \nu_z(\mathbf{x}_2, t + \delta t / 2) = -\frac{1}{\rho} \tilde{\partial}_z^+ p(\mathbf{x}, t + \delta t / 2), \tag{10c}$$

in which the operator δ_t is expressed in Eq. (7a); the operators $\tilde{\delta}_x^+$,





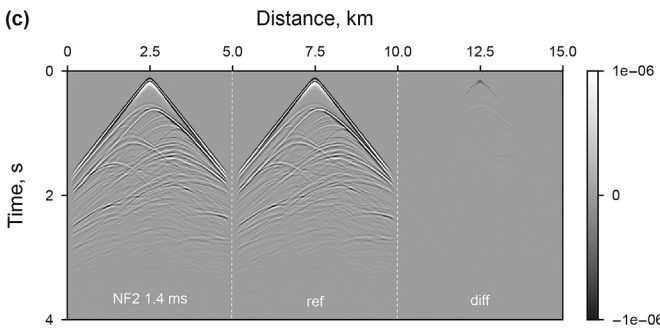


Fig. 10. Seismic records of NF2, PS, reference solution and their difference. (a) PS with time step 1 ms. (b) PS with time step 0.5 ms. (c) NF2 with time step 1.4 ms. The annotation "ref" and "diff" means reference solution and the difference between the reference solution and the method labeled at the left part of each subfigure. The reference solution is calculated by the conventional PS method with time step 0.001 ms. All methods adopt rank 4 for low-rank decomposition.

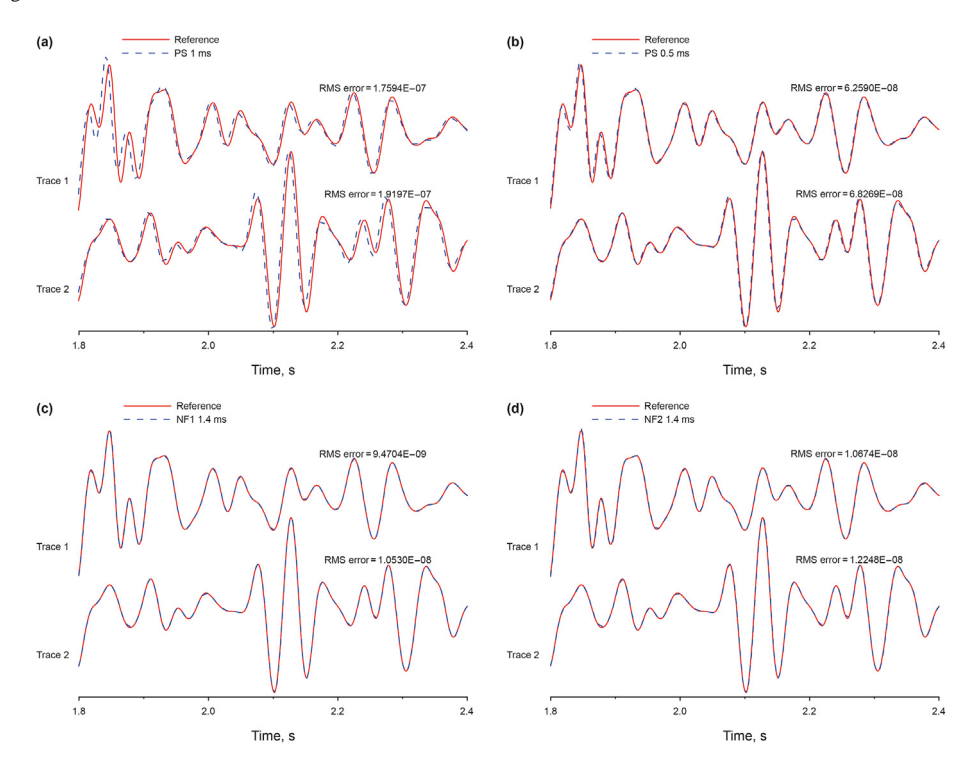


Fig. 11. Seismic traces from PS, NF1 and NF2. Traces 1 and 2 are located at x = 1.5 and 3.5 km, respectively. All methods adopt rank 4 for low-rank decomposition. (a) PS with time step 1 ms and reference solution; (b) PS with time step 0.5 ms and reference solution; (c) NF1 with time step 1.4 ms and reference solution; (d) NF2 with time step 1.4 ms and reference solution. The reference solution is calculated by the conventional PS method with time step 0.001 ms.

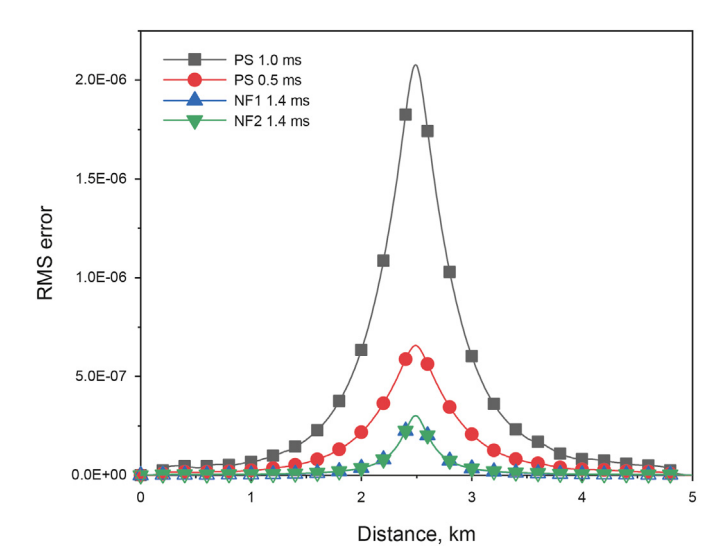


Fig. 12. RMS errors of the seismic records of PS, NF1 and NF2 in Figs. 9 and 10.

 $\tilde{\partial}_{x}^{-}$, $\tilde{\partial}_{z}^{+}$, $\tilde{\partial}_{z}^{-}$ and ∂_{s} can be expressed as

$$\tilde{\delta}_{\mathbf{x}}^{+}g(\mathbf{x},t) = \mathcal{F}^{-1}\left[e^{\mathrm{i}k_{\mathbf{x}}\delta\mathbf{x}/2}\widehat{\delta}_{\mathbf{x}}F[g(\mathbf{x},t)]\right],\tag{11a}$$

$$\tilde{\partial}_{\mathbf{x}}^{-}g(\mathbf{x},t) = \mathcal{F}^{-1}\left[e^{-\mathrm{i}k_{\mathbf{x}}\delta\mathbf{x}/2}\widehat{\partial}_{\mathbf{x}}F[g(\mathbf{x},t)]\right],\tag{11b}$$

$$\hat{\delta}_{z}^{+}g(\boldsymbol{x},t) = \mathcal{F}^{-1}\left[e^{ik_{z}\delta z/2}\widehat{\delta}_{z}F[g(\boldsymbol{x},t)]\right], \tag{11c}$$

$$\tilde{\partial}_{z}^{-}g(\mathbf{x},t) = \mathcal{F}^{-1}\left[e^{-\mathrm{i}k_{z}\delta z/2}\widehat{\partial}_{z}F[g(\mathbf{x},t)]\right],\tag{11d}$$

$$\partial_s g(\mathbf{x}, t) = \mathscr{F}^{-1} \left[\frac{e^{-b\delta t} - 1}{\delta t} F[g(\mathbf{x}, t)] \right].$$
 (11e)

Note that although the NF1 is in the discrete form, it is still the exact solution of Eq. (1) for the homogeneous case because it is derived all the way from Eq. (1) without any approximation. Particularly, when Q approximates $+\infty$, Eqs. (10a)-(10c) reduce to the exact k-space analytical solution for the lossless scalar wave simulation (Tabei et al., 2002). To validate the correctness of NF1 for the first-order viscoacoustic wave equation, we compare our numerical result with the analytical solution generated by the Green's function method (Carcione, 2007) in Fig. 1. It follows that the numerical results of our k-space formulation NF1 conform to the analytical solutions very well for a wide range of Q. The experiment demonstrates the correctness of our derivation.

In Fig. 2, we compare our viscoacoustic NF1 with the conventional pseudospectral (PS) method in the homogeneous case. It shows that the snapshots of the viscoacoustic PS suffer from the temporal dispersion, especially with the increase of the time step. By contrast, the snapshot of our viscoacoustic NF1 demonstrates no obvious dispersion effect despite using large time step.

For the homogeneous media, the velocity and Q are constants, and the pseudo-differential operator \sqrt{L} only varies with wavenumber \mathbf{k} . Eqs. (10a)-(10c) can be efficiently solved by the PS method and yield numerical dispersion free wavefields. However, for the heterogeneous media, the operator \sqrt{L} lies in the wavenumber-space $(\mathbf{k}-\mathbf{x})$ mixed-domain. As pointed out in Du et al. (2020), the exact representation of the mixed-domain operator by the phase-shift plus selection (PSPS) method can be prohibitively expensive. To deal with the issue, we use the low-rank matrix decomposition method (Engquist and Ying, 2009; Fomel et al., 2013) to approximate the operator \sqrt{L} , which has the form

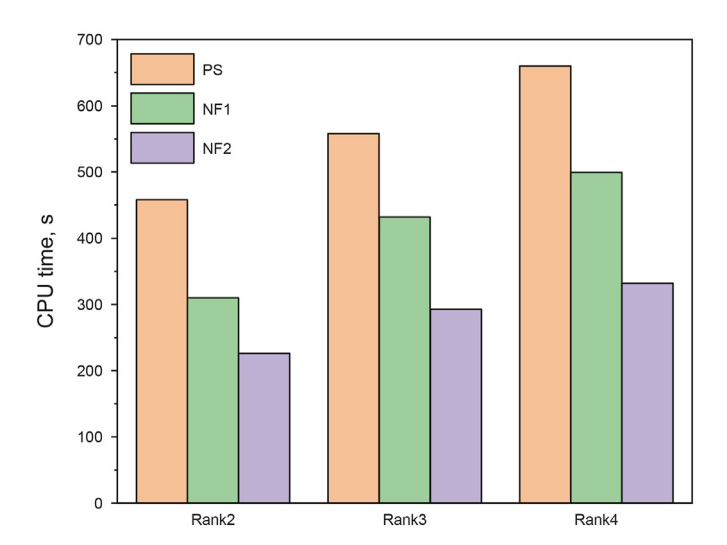


Fig. 13. CPU run times of PS, NF1 and NF2 for 4 s simulation. The time steps for rank 2, 3 and 4 are 1.2, 1.3 and 1.4 ms, respectively. The time step of PS method is 0.5 ms.

$$\sqrt{L} = \sqrt{L(\mathbf{x}, \mathbf{k})} \approx \mathbf{U}_{pm} \mathbf{V}_{mn} \mathbf{W}_{nq} = \mathbf{T}_{pn} \mathbf{W}_{nq},$$
 (12)

in which the dimension of matrix $L(\mathbf{x}, \mathbf{k})$ is $p \times q$, containing p rows space-related and q columns wavenumber-related information; the matrices $\mathbf{U}_{pm} = \mathbf{U}_{pm}(\mathbf{x}, \mathbf{k}_m)$ and $\mathbf{W}_{nq} = \mathbf{W}_{nq}(\mathbf{x}_n, \mathbf{k})$ are the m columns and n rows sub-matrices of $L(\mathbf{x}, \mathbf{k})$; \mathbf{V}_{mn} is the weighting matrix for \mathbf{U}_{pm} and \mathbf{W}_{nq} . With the matrix decomposition, the operator $\tilde{\delta}_{\mathbf{x}}^+$ in Eq. (11a) can be denoted as

$$\tilde{\boldsymbol{\partial}}_{x}^{+} g(\boldsymbol{x}, t) = \mathcal{F}^{-1} \left[e^{ik_{x}\delta x/2} \widehat{\boldsymbol{\partial}}_{x} F[g(\boldsymbol{x}, t)] \right]
\times \left[\approx \mathbf{T}_{pn} \mathcal{F}^{-1} \left\{ ik_{x} e^{ik_{x}\delta x/2} \mathbf{W}_{nq} g(\boldsymbol{k}, t) \right\}.$$
(13)

By using the low-rank method (Engquist and Ying, 2009; Fomel et al., 2013), the number of the inverse Fourier transform decreases from a large number p to a small number n, which is the rank controlling the accuracy of approximation. Similarly, one can approximate the operators $\tilde{\delta}_x^-$, $\tilde{\delta}_z^+$, $\tilde{\delta}_z^-$ and θ_s by the low-rank method (Engquist and Ying, 2009; Fomel et al., 2013) to enhance the efficiency.

2.3. New first-order staggered-grid formulation of viscoacoustic wave equation: formulation 2

Although the efficiency of the NF1 based k-space method is enhanced by the low-rank method (Engquist and Ying, 2009; Fomel et al., 2013) for the mixed-domain operators in the heterogeneous media, there are still too many mixed-domain operators in NF1. If one can reduce the number of the mixed-domain operators, the computational cost can be fundamentally reduced. In this section, we reach the goal by an alternative k-space formulation for the first-order viscoacoustic wave equation, and we name the formulation as new formulation 2 (NF2), which can be realized by reformulating Eq. (8) as

$$\frac{P(\mathbf{k}, t + \delta t/2) - P(\mathbf{k}, t - \delta t/2)}{\delta t}$$

$$= -\rho v^{2} (ik_{X}V_{X}(\mathbf{k}, t) + ik_{Z}V_{Z}(\mathbf{k}, t)) + \frac{P(\mathbf{k}, t - \delta t/2) \left(e^{-b\delta t} - 1\right)}{\delta t},$$
(14a)

$$\frac{V_{X}(\mathbf{k}, t + \delta t) - V_{X}(\mathbf{k}, t)}{\delta t} = -\frac{1}{\rho} \widehat{\vartheta}_{X}^{*} P(\mathbf{k}, t + \delta t / 2), \tag{14b}$$

$$\frac{V_z(\mathbf{k}, t + \delta t) - V_z(\mathbf{k}, t)}{\delta t} = -\frac{1}{\rho} \hat{\vartheta}_z^* P(\mathbf{k}, t + \delta t / 2), \tag{14c}$$

in which $P(\boldsymbol{k},t) = \frac{U(\boldsymbol{k},t+\delta t/2)-U(\boldsymbol{k},t-\delta t/2)}{\delta t}$, $V_X(\boldsymbol{k},t) = -\frac{1}{\rho}\widehat{\partial}_X^*U(\boldsymbol{k},t)$, $V_Z(\boldsymbol{k},t) = -\frac{1}{\rho}\widehat{\partial}_Z^*U(\boldsymbol{k},t)$, $\widehat{\partial}_X^* = \mathrm{i}k_XL$ and $\widehat{\partial}_Z^* = \mathrm{i}k_ZL$. The corresponding spacetime domain staggered-grid forms of NF2 are

$$\partial_t p(\mathbf{x}, t) = -\rho v^2 \left(\partial_X^- v_X(\mathbf{x}_1, t) + \partial_Z^- v_Z(\mathbf{x}_2, t) \right) + \partial_S p\left(\mathbf{x}, t - \frac{\delta t}{2}\right), \tag{15a}$$

$$\partial_t \nu_x \left(\mathbf{x}_1, t + \frac{\delta t}{2} \right) = -\frac{1}{\rho} \partial_x p \left(\mathbf{x}, t + \frac{\delta t}{2} \right), \tag{15b}$$

$$\partial_{t}\nu_{z}(\mathbf{x}_{2},t+\delta t/2) = -\frac{1}{\rho} \stackrel{\sim}{\partial}_{z}^{+} p(\mathbf{x},t+\delta t/2), \tag{15c}$$

in which the operators ∂_t , ∂_x^- and ∂_z^- are expressed in Eqs. (7a), (7d) and (7f), respectively; the operators ∂_x and ∂_z can be denoted as

$$\hat{\boldsymbol{\partial}}_{x} g(\boldsymbol{x}, t) = \mathcal{F}^{-1} \left[e^{i k_{x} t \hat{\boldsymbol{x}}} \hat{\boldsymbol{\partial}}_{x}^{*} F[g(\boldsymbol{x}, t)] \right], \tag{16a}$$

$$\stackrel{\smile}{\vartheta}_{z}g(\boldsymbol{x},t) = \mathcal{F}^{-1}\left[e^{\mathrm{i}k_{z}\delta z/2}\widehat{\vartheta}_{z}^{*}F[g(\boldsymbol{x},t)]\right]. \tag{16b}$$

Note that like NF1, NF2 can exactly reproduce the wave equation solution in Eq. (8) by eliminating the velocity variables, and thus NF2 can obtain dispersion free wavefield in the homogeneous case. To validate the correctness of our NF2, we make a quick test by adopting the analytical solution of Green's function (Carcione, 2007) in the homogeneous media. It can be observed in Fig. 3 that the modeled traces agree well with the analytical ones for different *Q*. These simple examples validate the correctness of our derivation for NF2.

In Fig. 4, we compare our NF1, NF2 and the conventional PS methods in the homogeneous cases. It follows that the snapshot of the conventional PS method shows significant phase advance in Fig. 4a, indicating strong temporal dispersion, while the snapshot of the NF2 method in Fig. 4b shows very clear wavefront. Fig. 4c compares the snapshot of the NF1 method with that of the NF2. It shows that the snapshot difference of two methods is almost invisible, which demonstrates the equally high accuracy of the NF1 and NF2 methods when compared with the PS method.

Note that the key merit of our NF2 is that it contains fewer mixed-domain operators than the NF1. The NF2 only contains 3 mixed-domain operators, while the NF1 includes 5 ones. For the homogeneous case, this difference is trivial because the mixed-domain operators reduce to the wavenumber domain ones, and the NF1 and the NF2 take the same computational cost. However, for the heterogeneous case, the NF2 takes fewer times Fourier transform operations than the NF1 because of reduction of the mixed-domain operators, and thus is more efficient. We will demonstrate this point in detail in the numerical examples section.

3. Numerical examples

In this section, we adopt two heterogeneous models to test the accuracy and efficiency of the conventional PS, NF1 and NF2 methods.

3.1. Two-laver model

First, we adopt a two-layer model to test the accuracy and efficiency of the conventional PS, NF1 and NF2 methods. The size of the velocity model is 600×600 with a grid spacing 20 m. The Pwave velocity is defined at a reference frequency 50 Hz. The velocities of the upper and lower layers are 2.6 km/s and 4 km/s, respectively. The interface of the model is at depth 6 km. The density is calculated by the empirical formula $ho = 310 v^{0.25}$. A 25 Hz Ricker wavelet is added at (x, z) = (6, 5) km. The rank parameter for three methods is 2. Fig. 5 compares the simulation accuracy of the PS, NF1 and NF2 methods by using the same time step. It can be observed that the snapshot of the conventional PS shows obvious dispersion effects because of discretization errors in time. By contrast, the snapshots of the NF1 and NF2 methods are nearly free from discretization errors. In Fig. 6, we increase the time step of the NF1 and NF2 methods to 3 ms. The snapshots of the two k-space methods remain accurate. The PS method breaks down because the stability condition is not satisfied when adopting such a time step. Therefore, we only display the snapshot of the PS method by a time step of 1 ms. One can observe that the PS method still suffers from weak discretization errors in time. In Fig. 7, we compare the CPU time for the PS. NF1 and NF2 methods under the comparable accuracy. It follows from Fig. 7 that the NF1 and NF2 methods are more efficient than the PS method, and the NF2 method takes less simulation time than the NF1 method.

3.2. Marmousi model

Second, we adopt the complex Marmousi velocity and Q models in Fig. 8 to test the accuracy and efficiency of the PS, NF1 and NF2 methods. The velocity is defined at the reference frequency 50 Hz. The density is calculated by the empirical formula $\rho = 310v^{0.25}$. The grid spacing is 10 m. A 25 Hz Ricker wavelet is added at (x, z) =(2.5, 0.1) km. The receivers are at the depth z = 0.2 km. We compare the accuracy of the NF1 and NF2 methods by their seismic records in Fig. 9. It shows that the difference between the two methods is almost invisible. Because of this feature, we only compare the PS method with the NF2 method in Fig. 10. We demonstrate that with the decrease of the time step, the discrepancy between the PS method and the reference solution decreases. The seismic record error of the NF2 method with time step 1.4 ms is smaller than that of the PS method with time step 0.5 ms. Then we extract the traces at x = 1.5 and 3.5 km from the seismic records in Fig. 11. These comparisons show that the traces of the PS method with time step 1 ms significantly deviate from the reference solution. Reducing the time step of the PS method to 0.5 ms decreases the discrepancy. However, the traces of PS method still do not match the reference solution very well, and the traces of the NF1 and NF2 methods match the reference solution better than those of the PS method. In Fig. 12, we further calculate the RMS error of the seismic records from the PS, NF1 and NF2 methods. The RMS error of different methods also demonstrates that the NF1 and NF2 methods with time step 1.4 ms are more accurate than the PS method with time step 1 ms or even 0.5 ms. Note that the conventional PS method for the viscoacoustic simulation breaks down when using the time step 1.4 ms because of the numerical instability. However, the NF1 and NF2 methods are still stable for such a time step. Last, we compare the modeling efficiency of the PS method with the NF1 and NF2

methods in Fig. 13. As demonstrated before, the NF1 and NF2 methods with time step 1.4 ms have higher accuracy than the PS method with time step 0.5 ms. Therefore, we only focus on the comparison using these parameters. The comparison demonstrates that the NF1 and NF2 methods are more efficient than the PS method. The NF2 takes less CPU time than the NF1 due to the reduction of the mixed-domain operators. Therefore, the NF2 method is the most efficient one among three methods.

4. Conclusion

We have developed two exact first-order k-space formulations for the fractional derivative based constant-Q viscoacoustic wave equation. Two new formulations can fully exclude the numerical dispersion error for the homogeneous media. We have compared two formulations with the conventional PS method by the homogeneous and heterogeneous examples, demonstrating that our new formulations are more accurate and stable than the PS method. Under the comparable accuracy, the new k-space formulations are more efficient than the PS method. In addition, our second kind of first-order k-space formulation is the most efficient one among three methods because of the reduction of the mixed-domain operators.

Acknowledgements

We thank anonymous reviewers for their constructive criticism of the paper. This research is supported by the National Natural Science Foundation of China (NSFC) under contract No. 42274147 and 41874144, and the Research Foundation of China University of Petroleum-Beijing at Karamay under contract No. RCYJ2018A- 01-001

Appendix A. Derivation for the k-space time marching form for the viscoacoustic case

In the appendix, we derive the exact k-space time marching form based on the dispersion relation of the viscoacoustic wave equation (Zhu and Harris, 2014). The $\mathbf{k} - \omega$ domain viscoacoustic wave equation can be expressed in the following alternative way:

$$(i\omega)^2 + bi\omega + c = 0, (A.1)$$

where $b=-v^2\tau|\pmb{k}|^{2\gamma+1}$ and $c=-v^2\eta|\pmb{k}|^{2\gamma+2}$. The variable $\mathrm{i}\omega$ has solutions

$$i\omega = \frac{-b \pm i\sqrt{4c - b^2}}{2}.$$
 (A.2)

Multiplying $\pmb{k}-\omega$ domain wavefield $U(\pmb{k},\omega)$ on both sides of the equation gives

$$i\omega U(\mathbf{k},\omega) = \frac{-b \pm i\sqrt{4c - b^2}}{2}U(\mathbf{k},\omega),$$
 (A.3)

which can be turned back into time domain as

$$\frac{\partial}{\partial t}U(\mathbf{k},t) - fU(\mathbf{k},t) = 0, \tag{A.4}$$

where $f = \frac{-b \pm i \sqrt{4c - b^2}}{2}$. Eq. (A.4) has analytical solution (Boyce et al., 2021)

$$U(\mathbf{k},t) = U(\mathbf{k},0)e^{ft}.$$
 (A.5)

From Eq. (A.5), we have

$$U(\mathbf{k}, t + \delta t) = U(\mathbf{k}, t)e^{f\delta t}, \tag{A.6}$$

$$U(\mathbf{k}, t - \delta t) = U(\mathbf{k}, t)e^{-f\delta t}, \tag{A.7}$$

and further have k-space formulation

$$= \frac{U(\mathbf{k},t)2\left(e^{-\frac{b}{2}\delta t}\cos\left(\frac{\sqrt{4c-b^2}}{2}\delta t\right)-1\right)}{\delta t^2} + \frac{U(\mathbf{k},t-\delta t)\left(1-e^{-b\delta t}\right)}{\delta t^2}.$$
(A.8)

Eq. (A.8) is the final k-space time marching form for the viscoacoustic case. One can reformulate the k-space time marching form as the first order forms in Eqs. (9) and (14), respectively.

Appendix B. Stability analyses for PS and two k-space methods of viscoacoustic case

In this part, we give brief analyses on the stability performance of the PS, NF1 and NF2 methods. For the PS method, transforming Eqs. (6a)-(6c) into the wavenumber-time domain and eliminating the velocity variables, we have

$$\frac{p(\mathbf{k}, t + \delta t) + p(\mathbf{k}, t - \delta t) - 2p(\mathbf{k}, t)}{\delta t^{2}}$$

$$= v^{2} \left(\tau |\mathbf{k}|^{2\gamma + 1} \frac{p(\mathbf{k}, t) - p(\mathbf{k}, t - \delta t)}{\delta t} + \eta |\mathbf{k}|^{2\gamma + 2} p(\mathbf{k}, t)\right),$$
(B.1)

which can be rewritten as the matrix recursive form as

$$= \frac{\frac{U(\boldsymbol{k},t+\delta t)-2U(\boldsymbol{k},t)+U(\boldsymbol{k},t-\delta t)}{\delta t^2}}{\frac{U(\boldsymbol{k},t)2\left(e^{-\frac{b}{2}\delta t}\cos\left(\frac{\sqrt{4c-b^2}}{2}\delta t\right)-1\right)}{\delta t^2}+\frac{U(\boldsymbol{k},t-\delta t)\left(1-e^{-b\delta t}\right)}{\delta t^2},}{(B.5)}$$

which can be rewritten as the matrix recursive form as

$$\begin{pmatrix}
U(\mathbf{k}, t + \delta t) \\
U(\mathbf{k}, t)
\end{pmatrix} = \begin{pmatrix}
2e^{-\frac{b}{2}\delta t}\cos\left(\frac{\sqrt{4c - b^2}}{2}\delta t\right) & -e^{-b\delta t} \\
1 & 0
\end{pmatrix} \times \begin{pmatrix}
U(\mathbf{k}, t) \\
U(\mathbf{k}, t - \delta t)
\end{pmatrix}.$$
(B.6)

To ensure stable recursion, the eigenvalue of the updating matrix should be less than 1 (Liu and Sen, 2009), which is equivalent to

$$\left(2e^{-\frac{b}{2}\delta t}\cos\left(\frac{\sqrt{4c-b^2}}{2}\delta t\right)\right)^2 - 4e^{-b\delta t} \le 0, \tag{B.7}$$

which can be simplified as

$$\cos^2\left(\frac{\sqrt{4c-b^2}}{2}\delta t\right) \le 1. \tag{B.8}$$

Inequality (B.8) is the stability condition for NF1 and NF2 methods. For homogeneous *Q* and velocity media, this inequality is

$$\begin{pmatrix} p(\boldsymbol{k},t+\delta t) \\ p(\boldsymbol{k},t) \end{pmatrix} = \begin{pmatrix} v^2 \Big(\tau |\boldsymbol{k}|^{2\gamma+1} \delta t + \eta |\boldsymbol{k}|^{2\gamma+2} \delta t^2 \Big) + 2 & -1 - \delta t v^2 \tau |\boldsymbol{k}|^{2\gamma+1} \\ 1 & 0 \end{pmatrix} \begin{pmatrix} p(\boldsymbol{k},t) \\ p(\boldsymbol{k},t-\delta t) \end{pmatrix}.$$
 (B.2)

To ensure stable recursion, the eigenvalue of the updating matrix should be less than 1, which is equivalent to (Zhu and Harris, 2014)

$$\delta t \leq -\frac{v^2 \tau |\boldsymbol{k}|^{2\gamma+1} + \sqrt{-2v^2 \eta |\boldsymbol{k}|^{2\gamma+2}}}{v^2 \eta |\boldsymbol{k}|^{2\gamma+2}}.$$
(B.3)

The stability condition in inequality (B.3) is inconvenient to use. It is reported (Zhu and Harris, 2014) that for the PS method, the stability condition of the viscoacoustic wave simulation is stricter than that of the acoustic one, which has the stability condition form as

$$\frac{v\delta t}{h} \le \frac{\sqrt{2}}{\pi} \approx 0.45. \tag{B.4}$$

The inequality (B.4) can be deemed as a necessary condition of the PS method for stable viscoacoustic wave simulation. For NF1 and NF2 methods, transforming Eqs. (10a)-(10c) and (14a)-(14c) into the wavenumber-time domain and eliminating the velocity variables, we have an unified expression

always satisfied, therefore the simulation is always stable. For heterogeneous media, the operator $\cos^2\left(\frac{\sqrt{4c-b^2}}{2}\delta t\right)$ is a mixed-domain operator, which can be approximated by the low-rank algorithm (Engquist and Ying, 2009; Fomel et al., 2013). Therefore, the stability condition depends on the approximation accuracy. It is hard to determine when the approximated operator $\cos^2\left(\frac{\sqrt{4c-b^2}}{2}\delta t\right)$ turns out to be larger than 1. Therefore, we only use the numerical examples to compare the stability performance of PS, NF1 and NF2 methods.

References

Aki, K., Richards, P.G., 2002. Quantitative Seismology. W. H. Freeman, New York. Alkhalifah, T., 2000. An acoustic wave equation for anisotropic media. Geophysics 65 (4), 1239–1250. https://doi.org/10.1190/1.1444815.

Berenger, J.-P., 1994. A perfectly matched layer for the absorption of electromagnetic waves. J. Comput. Phys. 114 (2), 185–200. https://doi.org/10.1006/jcph.1994.1159.

Berkhout, A.J., 2014a. An outlook on the future of seismic imaging, Part I: forward and reverse modelling. Geophys. Prospect. 62 (5), 911–930. https://doi.org/10.1111/1365-2478.12161.

Berkhout, A.J., 2014b. An outlook on the future of seismic imaging, Part III: joint migration inversion. Geophys. Prospect. 62 (5), 950–971. https://doi.org/ 10.1111/1365-2478.12158.

Blanch, J.O., Robertsson, J.O., Symes, W.W., 1995. Modeling of a constant Q: methodology and algorithm for an efficient and optimally inexpensive viscoelastic technique. Geophysics 60 (1), 176–184. https://doi.org/10.1190/1.1443744.

- Bojarski, N.N., 1982. The k-space formulation of the scattering problem in the time domain. J. Acoust. Soc. Am. 72 (2), 570–584. https://doi.org/10.1121/1.388038.
- Boyce, W.E., DiPrima, R.C., Meade, D.B., 2021. Elementary Differential Equations and Boundary Value Problems. John Wiley & Sons.
- Campillo, M., Plantet, J.-L., Bouchon, M., 1985. Frequency-dependent attenuation in the crust beneath central France from Lg waves: data analysis and numerical modeling. Bull. Seismol. Soc. Am. 75 (5), 1395–1411. https://doi.org/10.1785/ BSSA0750051395.
- Carcione, J.M., 2007. Wave Fields in Real Media: Wave Propagation in Anisotropic, Anelastic, Porous and Electromagnetic Media. Elsevier.
- Carcione, J.M., 2010. A generalization of the Fourier pseudospectral method. Geophysics 75 (6), A53–A56. https://doi.org/10.1190/1.3509472.
- Carcione, J.M., Cavallini, F., Mainardi, F., et al., 2002. Time-domain modeling of constant-Q seismic waves using fractional derivatives. Pure Appl. Geophys. 159 (7), 1719–1736. https://doi.org/10.1007/s00024-002-8705-z.
- Carcione, J.M., Kosloff, D., Kosloff, R., 1988. Viscoacoustic wave propagation simulation in the earth. Geophysics 53 (6), 769–777. https://doi.org/10.1190/1.1442512.
- Chen, H., Zhou, H., Li, Q.Q., et al., 2016. Two efficient modeling schemes for fractional Laplacian viscoacoustic wave equation. Geophysics 81 (5), T233—T249. https://doi.org/10.1190/geo2015-0660.1.
- Chen, J.B., Liu, H., 2004. Optimization approximation with separable variables for the one-way wave operator. Geophys. Res. Lett. 31 (6). https://doi.org/10.1029/2004G1019429
- Collino, F., Tsogka, C., 2001. Application of the perfectly matched absorbing layer model to the linear elastodynamic problem in anisotropic heterogeneous media. Geophysics 66 (1), 294–307. https://doi.org/10.1190/1.1444908.
- Day, S.M., Minster, J.B., 1984. Numerical simulation of attenuated wavefields using a Padé approximant method. Geophys. J. Int. 78 (1), 105–118. https://doi.org/10.1111/j.1365-246X.1984.tb06474.x.
- De Basabe, J.D., Sen, M.K., Wheeler, M.F., 2016. Elastic wave propagation in fractured media using the discontinuous Galerkin method. Geophysics 81 (4), T163—T174. https://doi.org/10.1190/geo2015-0602.1.
- Du, Q., Ba, J., Han, D., et al., 2020. A staggered-grid lowrank finite-difference method for elastic wave extrapolation. Ann. Geophys. 63 (3), DM329-DM329. https://doi.org/10.4401/ag-8197.
- Emmerich, H., Korn, M., 1987. Incorporation of attenuation into time-domain computations of seismic wave fields. Geophysics 52 (9), 1252–1264. https:// doi.org/10.1190/1.1442386.
- Engquist, B., Ying, L., 2009. A fast directional algorithm for high frequency acoustic scattering in two dimensions. Commun. Math. Sci. 7 (2), 327–345. https:// doi.org/10.4310/CMS.2009.v7.n2.a3.
- Firouzi, K., Cox, B., Treeby, B., et al., 2012. A first-order k-space model for elastic wave propagation in heterogeneous media. J. Acoust. Soc. Am. 132 (3), 1271–1283. https://doi.org/10.1121/1.4730897.
- Fomel, S., Ying, L., Song, X., 2013. Seismic wave extrapolation using lowrank symbol approximation. Geophys. Prospect. 61 (3), 526–536. https://doi.org/10.1111/ j.1365-2478.2012.01064.x.
- Fornberg, B., 1987. The pseudospectral method: comparisons with finite differences for the elastic wave equation. Geophysics 52 (4), 483–501. https://doi.org/10.1190/1.1442319.
- Gong, X., Du, Q., Zhao, Q., et al., 2018. Pseudo-analytical finite-difference elastic-wave extrapolation based on the k-space methodElastic k-space based PAFD scheme. Geophysics 83 (1), T1–T14. https://doi.org/10.1190/geo2017-0088.1.
- Hestholm, S., Ruud, B., 1998. 3-D finite-difference elastic wave modeling including surface topography. Geophysics 63 (2), 613–622. https://doi.org/10.1190/
- Igel, H., 2017. Computational Seismology: a Practical Introduction. Oxford University Press.
- Kjartansson, E., 1979. Constant Q-wave propagation and attenuation. J. Geophys. Res. Solid Earth 84 (B9), 4737–4748. https://doi.org/10.1029/JB084iB09p04737.
- Komatitsch, D., Martin, R., 2007. An unsplit convolutional perfectly matched layer improved at grazing incidence for the seismic wave equation. Geophysics 72 (5), SM155—SM167. https://doi.org/10.1190/1.2757586.
- Liu, H.-P., Anderson, D.L., Kanamori, H., 1976. Velocity dispersion due to anelasticity; implications for seismology and mantle composition. Geophys. J. Int. 47 (1), 41–58. https://doi.org/10.1111/j.1365-246X.1976.tb01261.x.
- Liu, Y., Sen, M.K., 2009. A new time-space domain high-order finite-difference method for the acoustic wave equation. J. Comput. Phys. 228 (23). https:// doi.org/10.1016/j.jcp.2009.08.027.
- McDonal, F., Angona, F., Mills, R., et al., 1958. Attenuation of shear and compressional waves in Pierre shale. Geophysics 23 (3), 421–439. https://doi.org/10.1190/1.1438489
- Moczo, P., Kristek, J., Gális, M., 2014. The Finite-Difference Modelling of Earthquake Motions: Waves and Ruptures. Cambridge University Press.
- Özdenvar, T., McMechan, G.A., 1996. Causes and reduction of numerical artefacts in

- pseudo-spectral wavefield extrapolation. Geophys. J. Int. 126 (3), 819–828. https://doi.org/10.1111/j.1365-246X.1996.tb04705.x.
- Qu, Y., Li, J., 2019. Q-compensated reverse time migration in viscoacoustic media including surface topography. Geophysics 84 (4), S201–S217. https://doi.org/ 10.1190/geo2018-0313.1.
- Qu, Y., Wang, Y., Li, Z., et al., 2021. Q least-squares reverse time migration based on the first-order viscoacoustic quasidifferential equations. Geophysics 86 (4), S283—S298. https://doi.org/10.1190/geo2020-0712.1.
- Robertsson, J.O., Blanch, J.O., Symes, W.W., 1994. Viscoelastic finite-difference modeling. Geophysics 59 (9), 1444–1456. https://doi.org/10.1190/1.1443701.
- Sun, J., Zhu, T., Fomel, S., 2015. Viscoacoustic modeling and imaging using low-rank approximation. Geophysics 80 (5), A103—A108. https://doi.org/10.1190/geo2015-0083.1.
- Tabei, M., Mast, T.D., Waag, R.C., 2002. A k-space method for coupled first-order acoustic propagation equations. J. Acoust. Soc. Am. 111 (1), 53–63. https:// doi.org/10.1121/1.1421344.
- Treeby, B.E., Cox, B.T., 2010. Modeling power law absorption and dispersion for acoustic propagation using the fractional Laplacian. J. Acoust. Soc. Am. 127 (5), 2741–2748. https://doi.org/10.1121/1.3377056.
- Virieux, J., 1986. P-SV wave propagation in heterogeneous media: velocity-stress finite-difference method. Geophysics 51 (4), 889–901. https://doi.org/10.1190/11442147
- Virieux, J., Operto, S., 2009. An overview of full-waveform inversion in exploration geophysics. Geophysics 74 (6), WCC1–WCC26. https://doi.org/10.1190/ 13238367
- Wang, J., Liu, Y., Zhou, H., 2021. Acoustic wave propagation with new spatial implicit and temporal high-order staggered-grid finite-difference schemes. J. Geophys. Eng. 18 (5), 808–823. https://doi.org/10.1093/jge/gxab053.
- Wang, J., Liu, Y., Zhou, H., 2022a. High temporal accuracy elastic wave simulation with new time-space domain implicit staggered-grid finite-difference schemes. Geophys. Prospect. https://doi.org/10.1111/1365-2478.13244.
- Wang, J., Liu, Y., Zhou, H., 2022b. A new linear optimized time-space domain spatial implicit and temporal high-order finite-difference scheme for scalar wave modeling. J. Appl. Geophys. 201, 104637. https://doi.org/10.1016/j.jappgeo.2022.104637.
- Wang, N., Zhu, T., Zhou, H., et al., 2020. Fractional Laplacians viscoacoustic wavefield modeling with k-space-based time-stepping error compensating scheme. Geophysics 85 (1), T1–T13. https://doi.org/10.1190/geo2019-0151.1.
- Wang, Y., Qu, Y., 2021. Q-compensated full waveform inversion for velocity and density. Explor. Geophys. 1–14. https://doi.org/10.1080/08123985.2021.1993059.
- Xing, G., Zhu, T., 2019. Modeling frequency-independent Q viscoacoustic wave propagation in heterogeneous media. J. Geophys. Res. Solid Earth 124 (11), 11568–11584. https://doi.org/10.1029/2019JB017985.
- Xu, J., Zhang, W., Chen, X., 2021. An optimized finite difference method based on a polar coordinate system for regional-scale irregular topography. Earthq. Sci. 34 (4), 334–343. https://doi.org/10.29382/eqs-2021-0022.
- Yoshimoto, K., Sato, H., Ohtake, M., 1993. Frequency-dependent attenuation of P and S waves in the Kanto area, Japan, based on the coda-normalization method. Geophys. J. Int. 114 (1), 165–174. https://doi.org/10.1111/j.1365-246X.1993.tb01476.x.
- Zhang, Y., Zhang, G., 2009. One-step extrapolation method for reverse time migration. Geophysics 74 (4), A29—A33. https://doi.org/10.1190/1.3123476.
- Zhou, H., Liu, Y., Wang, J., 2021a. Acoustic finite-difference modeling beyond conventional Courant-Friedrichs-Lewy stability limit: approach based on variable-length temporal and spatial operators. Earthq. Sci. 34 (2), 123–136. https://doi.org/10.29382/eqs-2021-0009.
- Zhou, H., Liu, Y., Wang, J., 2021b. Elastic wave modeling with high-order temporal and spatial accuracies by a selectively modified and linearly optimized staggered-grid finite-difference scheme. IEEE Trans. Geosci. Rem. Sens. 60, 3000122. https://doi.org/10.1109/TGRS.2021.3078626.
- Zhou, H., Liu, Y., Wang, J., 2022. Time-space domain scalar wave modeling by a novel hybrid staggered-grid finite-difference method with high temporal and spatial accuracies. J. Comput. Phys. 455, 111004. https://doi.org/10.1016/ j.jcp.2022.111004.
- Zhu, T., Carcione, J., Harris, J., 2013. Approximating constant-Q seismic propagation in the time domain. Geophys. Prospect. 61 (5), 931–940. https://doi.org/10.1111/ 1365-2478.12044.
- Zhu, T., Harris, J., 2014. Modeling acoustic wave propagation in heterogeneous attenuating media using decoupled fractional Laplacians. Geophysics 79 (3), T105–T116. https://doi.org/10.1190/geo2013-0245.1.
- Zhu, T., Harris, J.M., 2015. Improved seismic image by Q-compensated reverse time migration: application to crosswell field data, west Texas. Geophysics 80 (2), B61–B67. https://doi.org/10.1190/geo2014-0463.1.
- Zhu, T., Harris, J.M., Biondi, B., 2014. Q-compensated reverse-time migration. Geophysics 79 (3), S77–S87. https://doi.org/10.1190/geo2013-0344.1.
- Zou, Q., Huang, J., Yong, P., et al., 2020. 3D elastic waveform modeling with an optimized equivalent staggered-grid finite-difference method. Petrol. Sci. 17 (4), 967–989. https://doi.org/10.1007/s12182-020-00477-3.